Available online at www.sciencedirect.com
SCIENCE DIRECT®
International Journal of Heat and Mass Transfer 48 (2005) 3167–3175
International Journal of HEAT and MASS TRANSFER
www.elsevier.com/locate/ijhmt

Spray impingement cooling with single- and multiple-nozzle arrays. Part I: Heat transfer data using FC-72

A.G. Pautsch, T.A. Shedd *

University of Wisconsin-Madison, MFVAL, 1500 Engineering Drive, Madison, WI 53706-1609, USA

Received 1 January 2005; received in revised form 3 February 2005
Available online 20 April 2005

Abstract

With electronic packages becoming more dense and powerful, traditional methods of thermal energy removal are reaching their limits. One method of direct contact cooling capable of removing high heat fluxes while still being compact in size is spray impingement cooling, but its heat transfer behavior is not understood well enough to enable systematic, practical system design. This work presents the results of a large parametric study of spray cooling using a number of different nozzle patterns. It was found that nozzles that use the fluid most efficiently to remove thermal energy were limited by low peak heat fluxes and that the highest peak heat fluxes were obtained when phase change was avoided. Multiple nozzle arrays allowed for higher peak heat fluxes but used fluid inefficiently due to interactions between neighboring sprays. In general, the geometric pattern of the nozzle arrays had little effect on overall heat transfer performance.

Keywords: Spray cooling; Heat transfer; Critical heat flux

1. Introduction

The removal of very large heat fluxes is becoming a barrier to the technology roadmaps for microprocessors, power electronic modules, and many other applications incorporating microelectronic or microphotonic devices. In many of these applications, it is desirable that the thermal management system provide high rates of heat removal uniformly over a large area. Spray cooling is a promising candidate to address the thermal concerns of systems requiring high heat flux removal in a compact volume, as demonstrated by its successful commercial application in the Cray X1 vector supercomputers [1] and the numerous patents that have been granted for various spray cooling applications. However, application to future generations of high heat flux devices will require more uniform surface temperatures and higher peak heat fluxes than are available today.

In order to achieve high heat removal rates over large areas, a single, conical spray nozzle must be positioned relatively far from the heated surface to allow the spray to spread and cover the surface. To realize good spray coverage in a small volume, arrays of sprays may be used, as in the multi-chip module (MCM) used in the supercomputer application cited above. Despite the significant amount of research done on spray cooling using single nozzles, relatively little research has been done with multi-nozzle arrays. Pereira et al. [2] and Lin and Ponappan [3] studied the performance of arrays of sprays and found generally similar trends in heat

* Corresponding author.
E-mail address: shedd@engr.wisc.edu (T.A. Shedd).

0017-9310/$ - see front matter © 2005 Published by Elsevier Ltd.
doi:10.1016/j.ijheatmasstransfer.2005.02.012

Nomenclature

A	die surface area (cm^2)	η	cooling efficiency
c_p	liquid specific heat (kJ/kg K)	ρ	density (kg/m^3)
ΔT_{sat}	$T_{sat}-T_{in}$ (K)	ε	cooling effectiveness (J/ml)
h	local heat transfer coefficient ($W/cm^2 K$)	CHF	critical heat flux
h_{fg}	heat of vaporization (J/kg)	f	fluid
q''	heat flux (W/cm^2)	i	local
$\overline{Q}$	volumetric flow rate (ml/s)	in	fluid inlet
P_{res}	reservoir pressure (psia)	sat	saturation
T	temperature (°C)		

transfer performance as compared with single nozzle spray data such as those from Estes and Mudawar [4]. Horacek et al. [5] found that, for a given spacing between two sprays in an array, an optimum range of distances existed separating the sprays from the heater surface. If the sprays were too close, the heat transfer performance decreased due to the lack of area coverage. On the other hand, at too great of a distance, the number of drops per unit area of heated surface decreased, lowering heat transfer, in agreement with Mudawar and Estes [6]. Horacek et al. did not see any significant spray interaction effects. A later report by Lin et al. [7], however, indicates that penalties of over 30% in the critical heat flux (CHF) and heat transfer performance could be seen as the number of spray nozzles were increased to cover a large area.

This work presents the results of a detailed experimental investigation of the heat transfer performance of 10 different nozzle array patterns using Fluorinert FC-72 in a multi-chip module environment. Several significant observations are presented from these data. For example, it can be seen that single nozzles use fluid more efficiently than multiple nozzle arrays to remove thermal energy. However, peak heat fluxes are obtained when fluid is used least efficiently, i.e., when the thermal energy is removed via sensible heating of liquid with little or no evaporation. In addition, the peak heat flux is limited by de-wetting, or CHF, in regions of low fluid momentum, such as regions where multiple spray cones intersect, creating a stagnation zone.

2. Experimental apparatus

2.1. Test facility

The test stand consists of two parts: the fluid delivery system and the instrumentation system. The fluid used for testing is the fluorocarbon perfluo-rohexane, a dielectric fluid often used in electronics cooling applications and commonly known as the 3 M specialty fluid FC-72. The fluid delivery system is comprised of a fluid reservoir, magnetically coupled gear pump, filters (to remove particles, moisture, and gasses), and a flow meter, as well as the system manifold, spray cap, spray plate, and heat exchanger. A schematic of this facility is shown in Fig. 1. Further details of the test stand can be found in Pautsch's thesis [8].

The spray plate is oriented to deliver the fluid in an upwards direction such that the draining is gravity assisted, as shown in Fig. 1. Fluid leaving the spray cap passes through the system manifold into the heat exchanger unit, which is a fin-and-tube, liquid-to-air heat exchanger with copper fins and stainless steel tubes.

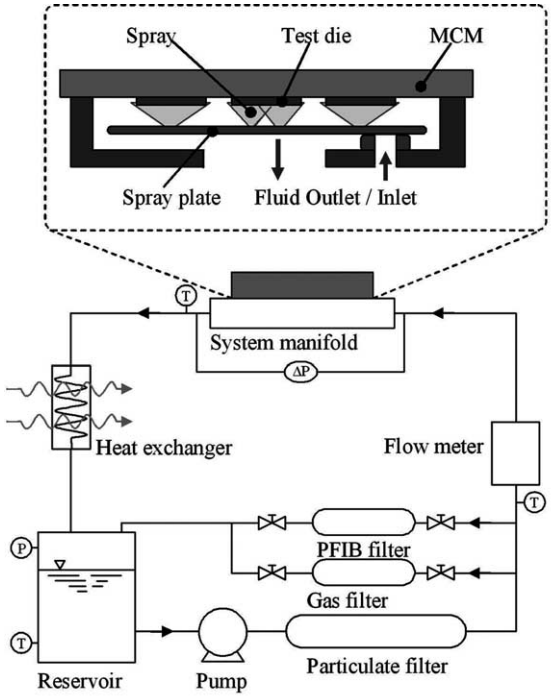

Fig. 1. Thermal test stand schematic and spray cap assembly.

Fluid leaving the heat exchanger unit is delivered to the reservoir. The entire fluid delivery system was manufactured from stainless steel except for the filter materials, two quick-disconnect fittings, O-ring seals, and short lengths of flexible tubing. Before initial testing, the entire fluid delivery system is evacuated to 28 inHg with a vacuum pump. Pre-conditioned fluid is pumped into the evacuated system. The pre-conditioning is performed with a Cray Inc. Fluid Conditioning Unit (FCU) so that the fluid used in this experiment is of the same quality and purity as that used in their production systems. The conditioning involves a thorough boiling and recondensing process to remove dissolved gasses, followed by filtration with a 5 μm filter. The system is then repressurized with pure nitrogen so that the system pressure is 26 °C at 101 kPa.

2.2. Nozzles

Tests in this study were performed with ten nozzle array designs. A nozzle array is defined as a nozzle, or set of nozzles, designated to cool one die. For each design, eight sets of nozzles are incorporated into a single spray plate designed and manufactured by Parker Hannifin Corporation. Plate design 10 is shown in Fig. 2 as an example. Each plate is divided into two sets of nozzles, labeled "A" and "B". The A nozzles are designed for lower flow rates and smaller area coverage at a given pressure differential than the B nozzles but are otherwise similar in structure and spray characteristics. The geometric and flow characteristics of each of the nozzle array designs are given in Table 1.

Each individual nozzle consists of a swirl chamber, two inlet slots, and a center jet to form a full spray cone [8]. Once installed in the tester, the nozzle arrays are located 6.8 mm under the center of each test die.

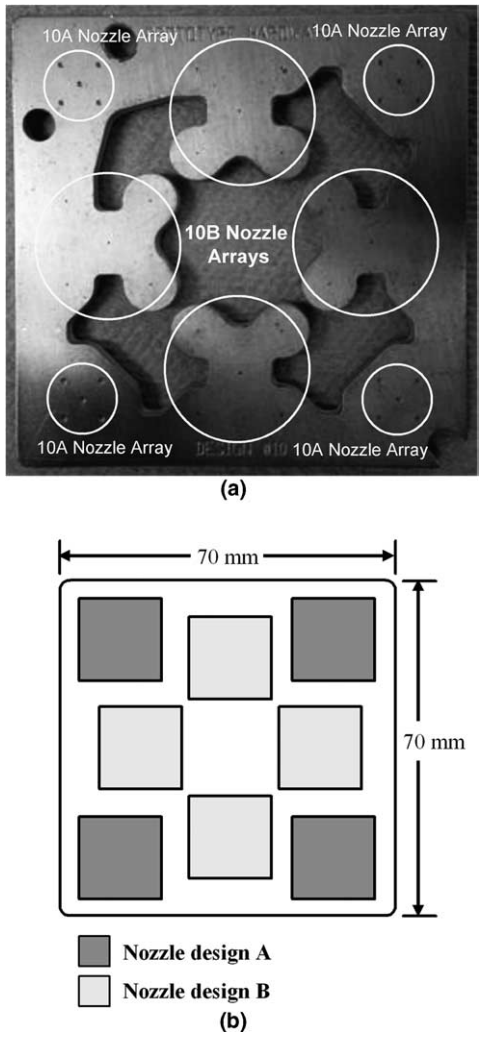

Fig. 2. (a) Spray plate design 10; (b) layout of heater elements on MCM.

2.3. Instrumentation

The instrumentation system includes all of the necessary electronic equipment to drive the fluid delivery system, to power the eight test dies, and to acquire any necessary measurements. The test dies are integrated circuits developed and built by IBM Corporation. Eight test dies are contained on one MCM, each measuring 15 mm on a side and square in shape (see Fig. 2). The MCM itself is 70 mm long by 70 mm wide by 5.25 mm thick. Each test die is built with eight temperature sensors (silicon diodes) integrated in the silicon that could be constantly monitored by the control software. The diodes were calibrated before use to ±0.2 °C uncertainty in a precision environmental chamber [8]. These devices measure the junction temperature of the die directly, which is the parameter of primary concern for electronics failure and reliability [9]. The surface temperature can be assumed to be close to the junction temperature due to the fact that the layers of silicon and silicon-dioxide on the surface between the junction plane and the free surface are conductive and extremely thin, on the order of microns; the temperature difference caused by these layers of material is much less than the uncertainty of the temperature measurement. The test stand is controlled by a Lab View program that records the die temperature distribution, the die power levels, and the state of the fluid delivery system, including the fluid flow rate, pressure, and temperature at several locations. The program also allows for control of the power level of all of the test dies, the pump, and the fans.

2.4. Operating procedure

The desired flow rate through the spray cap is set by adjusting the speed of the pump, after which the power

Table 1
Characteristics and flow rates of the nozzle arrays tested

Spray plate	Nozzle array A						Nozzle array B					
	No.	Pattern	Test pressure (kPa)				No.	Pattern	Test pressure (kPa)			
			103	172	241	301			103	172	241	301
			Flow rate (mL/s)						Flow rate (mL/s)			
0	1	·	0.67	0.86	1.01	1.13	4	∷	2.87	3.65	4.32	4.83
1	1	·	0.38	0.48	0.55	0.60	4	∷	2.13	2.69	3.12	3.40
10	5	⁙	0.45	0.54	0.65	0.73	5	⁙	2.09	2.54	3.06	3.43
11	2	⁘	0.12	0.15	0.17	0.19	9	⁞⁞	1.09	1.31	1.54	1.69
13	3	⁘	0.39	0.48	0.56	0.63	16	⁞⁞	2.32	2.85	3.35	3.75

Flow rates are per die.

supplies are adjusted to the desired starting power level. The fluid is then heated, if needed, from room temperature to 26 °C. A fluid testing temperature of 26 °C was chosen so that at 1 atm system absolute pressure (P_{res}) there would be approximately 30 degrees of subcooling. Fans mounted to the heat exchanger are controlled to maintain a constant fluid inlet temperature. The dies are held at the starting power level for 30 seconds to ensure that the system is in steady state and that critical heat flux has not occurred before a data point is recorded. After each data point is recorded, the die power is increased by 5 W, and after waiting thirty seconds, a new data point is recorded. When de-wetting (CHF) is detected by a run-away temperature sensor, the power level is decreased by 10 W and the testing is resumed using 1 W power increments to give a more accurate indication of the critical heat flux. Critical heat flux is defined as the highest heat flux that could be maintained with a stable surface temperature. When CHF is reached, the surface temperature will rise quickly as the system transitions to liquid film boiling.

Test results are presented as a function of the test pressure (ΔP_{cap}) instead of the flow rate because multiple nozzle designs are incorporated into each spray nozzle plate; it is impossible to set the flow rate of each individual nozzle. However, the average flow rate of each nozzle design per die is given in Table 1. The test pressure differentials chosen were 103, 172, 241, and 310 kPa (15, 25, 35, and 45 psi), which give a range of flows from 0.12 ml/s to 4.83 ml/s per die for the nozzle patterns used in this study. The minimum pressure of 103 kPa was chosen to ensure a high-quality spray for all nozzles. Two of the nozzle designs (0A and 0B) were run at a wider range of pressure differentials ranging from 34 to 310 kPa.

3. Results

3.1. Cooling effectiveness

A commonly cited performance characteristic of a nozzle design is the critical heat flux. This is found experimentally by raising the power levels of the thermal dies slowly until a temperature instability develops at the heater surface. This instability is indicated by a rapid rise in the surface temperature corresponding to the transition to de-wetting of the surface. Measurements of CHF were made at four flow conditions for each of the nozzle array designs. Values of CHF as high as 77.8 W/cm^2 were measured.

Critical heat flux is not necessarily the best standard on which to compare nozzle designs; nozzles are designed to match the amount of fluid used to the heat load. An unbiased parameter that accounts for the varying levels of fluid required for each nozzle design is the cooling effectiveness (ε) given in Eq. (1). Here, A is the die surface area, $\overline{Q}$ is the volumetric flow rate, and q'' is the heat flux. The units of the parameter simplify to J/ml.

$$\varepsilon = \frac{q''A}{\overline{Q}} \tag{1}$$

Fig. 3 presents CHF on the right axis versus the cooling effectiveness ε. The values of CHF are the solid symbols on the figure. A definite trend is seen with all of the

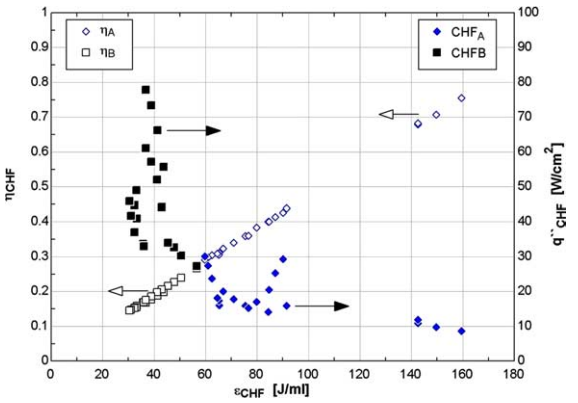

Fig. 3. Cooling efficiency and critical heat flux versus cooling effectiveness.

nozzles. Nozzles that are able to remove the most energy per unit of volumetric flow rate have very low critical heat fluxes: i.e., not enough fluid is delivered to remove large heat loads. In flow conditions where higher levels of CHF are achieved, the effectiveness values are lower. For the same amount of energy to be removed, a much larger amount of fluid is required. The trend seems to asymptote at approximately 30 J/ml. For nozzle designs of this type and their corresponding spray interactions, this appears to be the limit of effectiveness for high heat flux removal. Therefore, from these data, when designing a spray cooling nozzle for high maximum heat fluxes, a recommended flow rate should correspond to an ε-value of 40 J/ml or less.

3.2. Cooling efficiency

The effect that subcooling the fluid has on the system performance is not well understood, and the amount of evaporation that takes place in the liquid film during spray cooling is largely unknown or misunderstood. To take into effect these two parameters, a dimensionless efficiency value has been used to characterize nozzle designs [4]. The efficiency, shown in Eq. (2), is a ratio of the total heat load removed to the total heat capacity of the fluid, including the heating of the fluid from a subcooled state to saturation (sensible heat) and the complete vaporization of the liquid at saturation (latent heat). In this equation, c_p is the liquid specific heat, ΔT_{sat} is the level of subcooling, and h_{fg} is the heat of vaporization. A value of $\eta = 1$ corresponds to a fluid packet completely evaporating from the surface, which is the theoretical upper bound of η. This assumes that conduction through the die and radiative heat transfer are negligible compared to the rate of heat removal by the fluid, which are commonly accepted assumptions in spray cooling.

$$\eta = \frac{q'' A}{\overline{Q}\rho_{\text{f}}(c_p \Delta T_{\text{sat}} + h_{\text{fg}})} \tag{2}$$

The values of η obtained at CHF ($\eta_{\max}$) in the experiments are presented in Fig. 3 (left axis) and can be seen to range from 0.145 to 0.755 for the flows studied. Nozzle design 11A had significantly higher values of η than any of the other designs, meaning that much more of the fluid delivered to the surface underwent a phase change. All of the tests run in this study attempted to maintain the same level of subcooling ΔT_{sat}. The fluid could not undergo a phase change until this subcooling was overcome. The value of η required for this to occur ($\eta_{1\phi}$) is given in Eq. (3), the efficiency of a single-phase system. For the tests performed, it was found that $\eta_{1\phi} \approx 0.20$–$0.28$.

$$\eta_{1\phi} = \frac{\overline{Q}\rho_{\text{f}} c_p \Delta T_{\text{sat}}}{\overline{Q}\rho_{\text{f}}(c_p \Delta T_{\text{sat}} + h_{\text{fg}})} \tag{3}$$

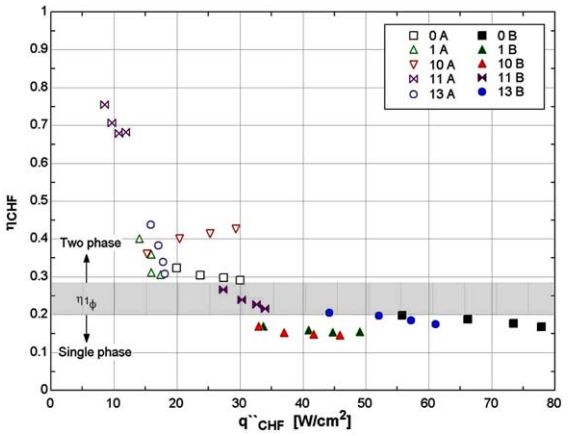

Fig. 4. Efficiency versus CHF for all nozzle designs.

As can be seen in Fig. 3, the plot of η versus ε generates a straight line. This is to be expected as η is a dimensionless form of ε. The slope of this line can be determined to be $\rho_{\text{f}}(c_p \Delta T_{\text{sat}} + h_{\text{fg}})$, which is a function only of the fluid properties at the test conditions. The fact that the line is linear demonstrates that the fluid inlet conditions were indeed maintained throughout testing. In addition, it is seen that designs with high efficiencies have lower values of CHF; alternatively, nozzle designs that achieve high levels of CHF rely less on phase change.

A plot of the efficiency at CHF ($\eta_{\max}$) versus CHF is shown in Fig. 4. The marked band of values represents the approximate range of η at which the single phase ends. Nozzle designs that rely less on multi-phase heat transfer are seen to obtain higher values of CHF. Some of the B nozzle designs, in fact, do not reach $\eta = \eta_{1\phi}$ before reaching CHF. This is likely because η is based on an average of temperatures over the entire die and not on local values. In the multiple-nozzle arrays, as all of the B nozzle designs are, there could exist a stagnation region in the liquid film at the surface where the interaction of the flows from different nozzles traps fluid in the center of the die between the nozzles. As the fluid outside of these stagnation regions is pushed off by incoming droplets, the fluid in the stagnation region locally undergoes a significant amount of phase change and reaches critical heat flux. If this is what is occurring, then a lower local heat transfer coefficient should be seen in the center locations of the B nozzle designs.

3.3. Heat transfer coefficient

Because temperature measurements were taken at 8 locations on the thermal test dies, a heat transfer coefficient distribution can be estimated spatially over the surface. The heat transfer coefficient at the ith location, h_i is calculated using

$$h_i = \frac{q''}{T_i - T_{\text{in}}}, \tag{4}$$

where T_i is the temperature of the ith sensor and T_{in} is the inlet liquid temperature. A local heat transfer coefficient using the local liquid temperature cannot be calculated at this time because the local liquid film temperature is not yet known. Instead, Eq. (4), where the temperature of the incoming fluid droplets is used for the temperature difference, is commonly used [10]. To simplify the data analysis, the eight heat transfer coefficients are averaged into three groups: center, corner, and quadrant centers. Each nozzle array was repeated four times per spray plate, so four of the eight test dies were cooled by each nozzle design. Therefore, the values of heat transfer coefficients presented here are not only an average of the various locations on a single die, but are also an average of the four dies. Although some local information is lost in this scheme, the larger number of samples increases the statistical reliability of the reported values.

When the data for the heat transfer coefficients were analyzed, it was discovered that, for the B nozzle designs, the highest heat transfer coefficients were always found at the corners of the dies. The B nozzle designs have nozzle arrays that cover a greater percentage of the entire die surface. Since most of the fluid on the surface is in a spray impact region, it tends not to heat up as much before it reaches the edge of the die as it would for a single nozzle flow, such as the 0A design. The flow from the B nozzle designs also tends to create a region in the inner area of the die where flows from multiple sprays come together into a stagnation region. This trend is not seen in the A nozzle designs, which show very little spatial distribution in temperature for some designs and more of a random pattern with others.

To gain a better understanding of the role that the heat transfer coefficient plays in CHF, a plot of the local heat transfer coefficient at CHF versus efficiency is presented in Fig. 5(a). This figure shows that, for B nozzle designs, the heat transfer coefficient sharply drops at a value of $\eta \approx 0.155 - 0.175$. It was stated earlier that the efficiency value corresponding to the end of the single-phase regime ($\eta_{1\phi}$) was calculated by Eq. (3) to be $\approx$0.25. Fig. 5 demonstrates the differences in performance characteristics between nozzle designs that primarily use single-phase cooling versus those that rely on two-phase heat removal. There is clearly a difference in the behavior of the liquid film for these two regions.

When the A nozzle designs were analyzed, a clearer trend than that found in the B nozzle designs was observed. Fig. 5(b) is a graphical representation of the findings. It is seen that the heat transfer coefficient drops off sharply at $\eta = 0.3$. As the efficiency increases, the heat transfer coefficient continues to decrease. The anomaly in this data set is nozzle array design 0A (a 5-nozzle array). All other designs have a decreasing trend, but design 10A increases with increasing efficiency after passing through a minimum. These results show that the cooling mechanism for this design is again different than the other nozzle designs. This nozzle design is worthy of further investigation. If the trend continues, it shows great promise for removing very high heat loads, because adding more fluid to it allows it to remove more heat from the surface where in other designs, less heat is removed.

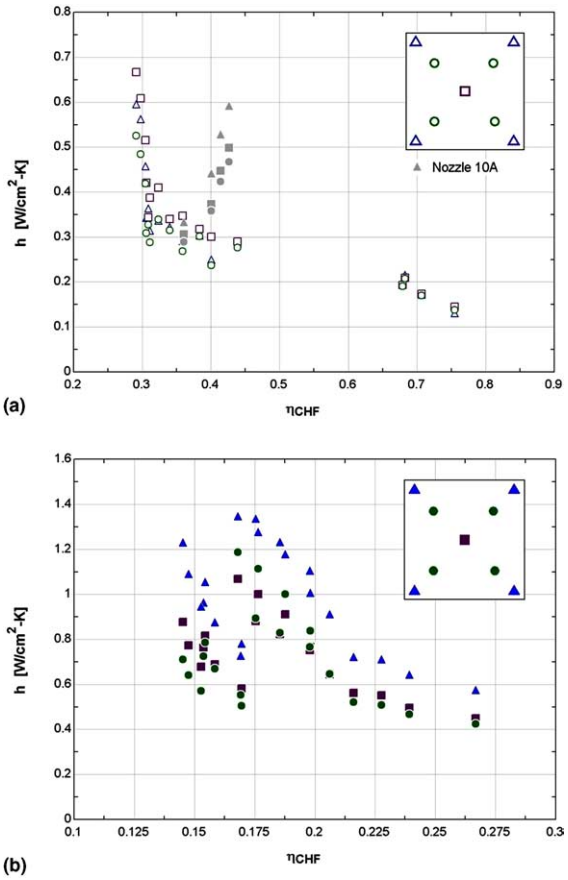

Fig. 5. Heat transfer coefficient versus efficiency at critical heat flux for A nozzle designs (a) and B nozzle designs (b).

Previous figures in this section have only shown the heat transfer coefficient at CHF. The heat transfer coefficients at heat loads leading up to CHF are shown in Fig. 6. Part (a) of this figure shows the heat transfer coefficients at the corner, center, and quadrant center regions plotted versus heat flux for nozzle 0A at a flow rate of 0.67 ml/s. The figure shows that the heat transfer coefficient for this nozzle was the highest at the center of the die. In both the center and the quadrant center regions, the heat transfer coefficient increased with the heat load. This occurred initially for the corner regions until approximately 17.5 W/cm^2, where the heat transfer

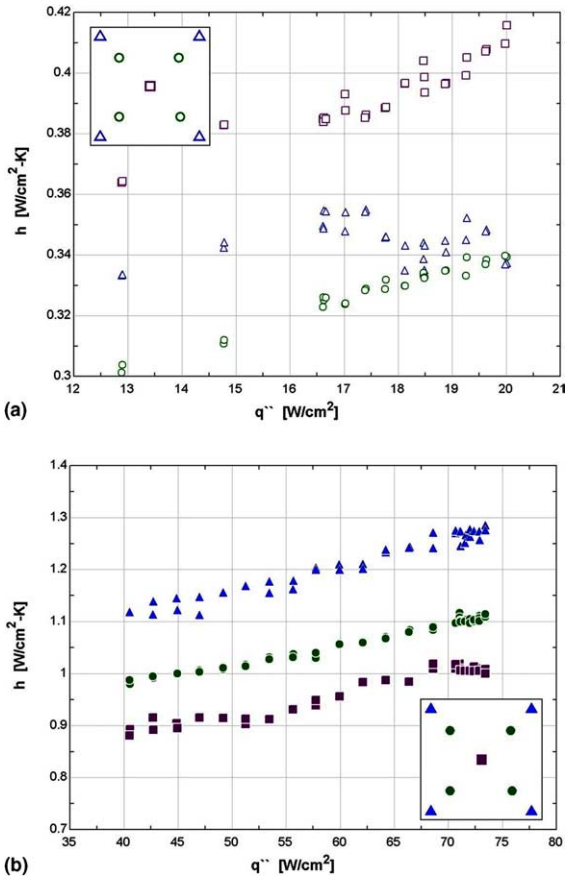

Fig. 6. Heat transfer coefficient versus heat flux for nozzle design 0A at 15 psid (a) and 0B at 35 psid (b).

coefficient began to decrease. At the critical heat flux, the corners became the poorest performing area with respect to the heat transfer coefficient. Using the temperature data, it was found that for nozzle 0A, CHF occurred at one corner of the die, the area that corresponds to the lowest heat transfer coefficient. A possible cause of this is the onset of nucleate boiling at the corners of the dies, which could lead to critical heat flux. As the flow rate increases, the onset of CHF is delayed.

A similar phenomenon is seen in the center region of the die when nozzle design 0B is examined at flow rate of 4.32 ml/s, as shown in Fig. 6(b). The center has the lowest heat transfer coefficient throughout testing. All of the curves are slowly increasing with increasing heat flux until 70 W/cm^2. At this heat load, the heat transfer coefficient at the center of the dies begins to decrease until CHF is reached. The change in the trend of the heat transfer coefficient is much more subtle for this design than for the single nozzle. The local temperature data consistently show that the dies would reach CHF in the center region with nozzle 0B. It is likely that the poor performance at the center of the die is due to the interaction of the sprays in this region.

Fig. 7 shows the heat transfer coefficient versus the heat flux for all of the flow rates tested using nozzles 0A and 0B. In the figure, the die average heat transfer coefficient is plotted instead of the separate values from the three regions. The average heat transfer coefficient is simply the average of the local heat transfer coefficient at the eight measured locations on the die. Two additional lines are shown on the figures as well: CHF for all tests at different flow rates and the point at which the average temperature of the die was measured to be 80 °C. This temperature is a common recommendation for the maximum junction temperature at which computer chips should be operated for reliability [9].

Part (a) of Fig. 7 shows the results for nozzle design 0A. The figure shows that the average heat transfer coefficient for each test run has approximately the same trend with respect to CHF as the other test runs; the slope of all the lines are very nearly the same. The line representing CHF is also very linear for all test runs,

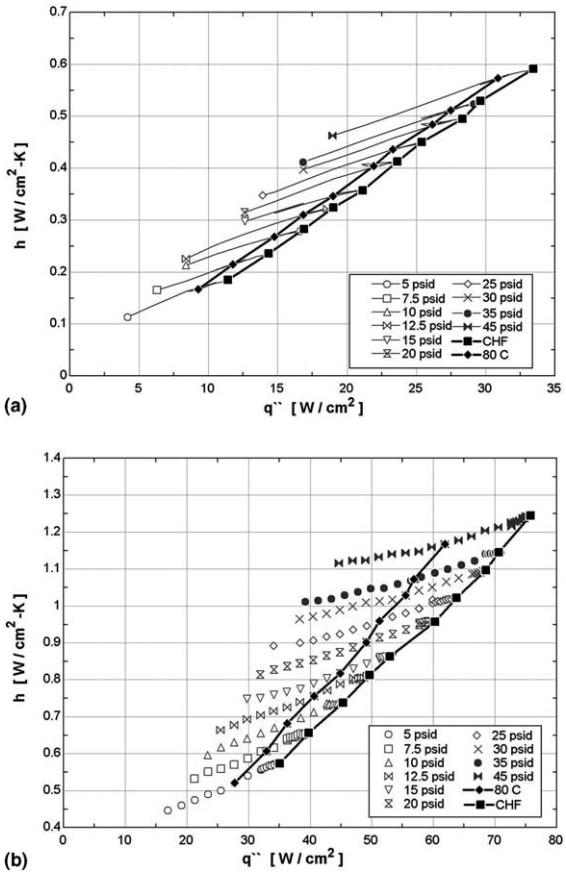

Fig. 7. Heat transfer coefficient versus heat flux for 0A (a) and 0B (b).

as is the 80° line. This makes CHF very easy to model and predict for any given flow rate. Also, it is interesting that the distance between the 80 °C line and the CHF line remains the same for all tests. This could be interpreted to mean that very little is changing in the behavior of the liquid film on the heater surface as the heat load is increased.

Part (b) of Fig. 7 is a plot for nozzle 0B, showing the same linearity for the CHF line and for the 80 °C line as the previous figure. However, the two lines are not parallel for this nozzle design. As the flow rate is increased, the onset of CHF increases faster than the constant temperature (80 °C) point, and the distance between the two curves grows. It would seem that the behavior of the liquid film that leads to CHF is suppressed at higher flow rates, as demonstrated by the larger distance between the two curves. This may be due to the fact that an increasing number of droplets are impacting the film with a velocity and frequency high enough to suppress surface nucleation, or to remove nucleate bubbles that form before they are allowed to fully grow, thereby prolonging the onset of critical heat flux.

4. Summary

The designs tested were arrays ranging from 1 to 16 nozzles of swirl-chamber type pressure atomizers. Some regions of the die perform better than others due to the patterns of the flow from the nozzles and the resulting behavior of the thin liquid film. The performance of the design is limited by the worst performing area of the die, as was shown in Fig. 6. In multiple-nozzle designs, this often occurs at the center region of the die due to flow interactions from neighboring nozzles. In single-nozzle arrays, critical heat flux first occurs at the edges of the die, where there is not a continual addition of fresh, cooler fluid. Also, less mixing of the film occurs there due to the lack of droplets perturbing the free surface of the film.

For the styles of nozzles tested, it was also discovered that systems that could achieve higher levels of critical heat flux relied less on the multi-phase component of heat transfer; rather, the designs are limited by the multi-phase component. Fig. 4 shows that the nozzle designs that removed higher heat loads reached critical heat flux before the point at which the die surface, on average, should achieve nucleate boiling. Nucleate boiling occurs locally in some areas sooner than others, but the latent heat capacity of the fluid cannot be used without triggering CHF.

Fig. 3 shows a further relationship between critical heat flux and nozzle performance. The figure illustrates that designs that make very effective use of the fluid being delivered are not able to achieve high levels of critical heat flux. Designs that could remove large amounts of energy from the die seemed to reach a performance limit of $\varepsilon = 40$ J/ml. This is a possible design parameter for future developments of spray cooling designs using full-cone nozzles. A maximum possible effectiveness of a nozzle design is implied in Fig. 3. This value can be found by dividing Eq. (2) by Eq. (1). For the test conditions used in this study, the thermal capacity of the designs was calculated to be 204.6 J/ml. This value is a function of the fluid properties and the amount of subcooling used (30 °C).

One set of nozzles tested, nozzle 10A, did not exhibit the same behavior as the other nine nozzles. The effectiveness values for this design lie between 76 and 90 J/ml as shown in Fig. 3, where CHF increases with increasing effectiveness.

This nozzle design, as shown in Table 1, is a low flow rate array of five nozzles. It is possible that the center nozzle adds enough fluid to cause the stagnation region of the film not to form. Note that the nozzle with this same geometrical pattern but wider nozzle spacing, nozzle 10B, did no show the same behavior. Thus, although the 10A design shows promise for future development, the comparison with the 10B design suggests that there is significant sensitivity of the heat transfer performance to nozzle spacing and geometry.

Acknowledgement

The authors gratefully acknowledge the financial support of the University of Wisconsin Office of University-Industry Relations, Robert Bolz, and Cray, Inc. Contributions of spray characterization from Parker Hannifin Corp. are also appreciated. The authors thank Natalie Meagher for gathering data and Prof. Greg Nellis for many helpful comments and discussions.

References

[1] G. Pautsch, An overview on the system packaging of the CRAY SV2 supercomputer, in: Proceedings of IPACK'01, The Pacific Rim/ASME International Electronic Packaging Technical Conference and Exhibition, ASME, 2001, pp. 617–624.

[2] R.H. Pereira, S.L. Barga, J.A.R. Parise, Comparing single phase heat transfer to arrays of impinging jets and sprays, in: Proceedings of IMECE2002, New Orleans, LA, USA, 2002, Paper IMECE2002-32531.

[3] L. Lin, R. Ponnappan, Heat transfer characteristics of spray cooling in a closed loop, Int. J. Heat Mass Transfer 46 (20) (2003) 3737–3746.

[4] K.A. Estes, I. Mudawar, Comparison of two-phase electronic cooling using free jets and sprays, Trans. ASME: J. Electron. Packag. 117 (1995) 323–332.

[5] B. Horacek, K.T. Kiger, J. Kim, Single nozzle spray cooling heat transfer mechanisms, Int. J. Heat Mass Transfer 48 (2005) 1425–1438.

[6] I. Mudawar, K.A. Estes, Optimizing and predicting CHF in spray cooling of a square surface, J. Heat Transfer 118 (1996) 672–679.
[7] L. Lin, R. Ponnappan, K. Yerkes, B. Hager, Large area spray cooling, in: 42nd AIAA Aerospace Sciences Meeting and Exhibit, Reno, Nevada, USA, 2004, pp. 10838–10843.
[8] A.G. Pautsch, Heat transfer and film thickness characteristics of spray cooling with phase change, Master's thesis, University of Wisconsin-Madison, Madison, Wisconsin, 2004.
[9] J.D. Parry, J. Rantala, C.J.M. Lasance, Enhanced electronic system reliability—Challenges for temperature prediction, IEEE Trans. Comp. Packag. Technol. 25 (4) (2002) 533–538.
[10] I. Mudawar, W.S. Valentine, Determination of the local quench curve for spray-cooled metallic surfaces, J. Heat Treatment 7 (1989) 107–121.